Near-Field Angle and Distance Estimation for Extremely Large UPA Systems

Hyeonjin Chung, Sunwoo Kim, Andrea Conti, and Moe Z. Win

Abstract—Due to the multi-dimensional search in the near-field (NF), the excessive computational burden has become one of the major problems. To address this issue, this paper proposes a computationally efficient angle and distance estimation algorithm for extremely large uniform planar array (UPA) systems. To reduce computation, the proposed algorithm decouples 3D search into a series of 2D search and 1D search. The 2D search estimates the azimuth and elevation, followed by the 1D search that estimates the distance. While the proposed algorithm brings significant improvement in computational complexity, the estimation of the proposed algorithm is guaranteed to be accurate as long as the distance between the receiver and transmitter (or scatterer) exceeds a specific threshold. For UPAs, we establish that this threshold is around a quarter of the Rayleigh distance. The simulation results demonstrate that the proposed algorithm has a superior accuracy-complexity trade-off compared to existing works.

Index Terms—Near-field effect, channel estimation, mmWave/THz communication, Rayleigh distance, massive MIMO

I. Introduction

As the demand for larger throughput continues to grow, the carrier frequency, as well as the number of antenna elements, have been increasing rapidly [1], [2]. When the system deploys the large antenna array, the NF effect is non-negligible since Rayleigh distance, the criteria that discriminate between far-field (FF) and NF, is proportional to the size of the antenna array [3]. Although the NF effect poses a challenge for channel estimation, it brings a new opportunity for ranging, which can contribute to the advancement of localization and location-aware communications [4]–[8].

To estimate the channel in the NF, the curvature of the spherical wavefront needs to be considered. Due to this nature, not only the angle, but the distance between the transmitter

The fundamental research described in this paper was supported, in part, by the National Research Foundation of Korea under Grant NRF-2023R1A2C3002890 and Grant RS-2024-00337368, by the European Union under the NextGenerationEU Italian NRRP PE00000001 program RESTART, by the National Science Foundation under Grant CNS-2148251, by the federal agency and industry partners in the RINGS program, and by the Robert R. Taylor Professorship.

Hyeonjin Chung is with the Wireless Information and Network Sciences Laboratory, Massachusetts Institute of Technology, Cambridge, MA 02139 USA (email: hyeonjin@mit.edu).

Sunwoo Kim is with the Department of Electronics and Computer Engineering, Hanyang University, Seoul, 04763, South Korea (email: remero@hanyang.ac.kr).

Andrea Conti is with the Department of Engineering and CNIT, University of Ferrara, 44122 Ferrara, Italy (email: a.conti@ieee.org).

Moe Z. Win is with the Laboratory for Information and Decision Systems (LIDS), Massachusetts Institute of Technology, Cambridge, MA 02139 USA (email: moewin@mit.edu).

and receiver affects the steering vector [9]–[14]. However, the problem of NF channel estimation is excessive computation time that is induced by a multidimensional search for angle and distance estimation [12], and this problem becomes more severe in UPA systems [11]. The algorithms in [12], [13] effectively reduce the computation without affecting the angle and distance estimation performance. However, they require the inter-antenna spacing smaller than a quarter-wavelength to prevent ambiguous estimation. This limitation is critical in practice since the antenna array is designed to have a spacing of more than half-wavelength [15]. The algorithm in [14] also aims to reduce the computational complexity. However, it only exploits one column of UPA for estimation, thereby suffering from performance degradation.

In this paper, we propose a computationally efficient NF angle and distance estimation algorithm that does not suffer from the constraints of existing works. The proposed algorithm does not require inter-antenna spacing of less than a quarter-wavelength to avoid ambiguous estimation. Moreover, the proposed algorithm leverages the entire antenna elements, which makes the estimation robust to noise and better capture the curvature of the wavefront. However, the proposed algorithm requires a specific condition to guarantee accurate estimation. We reveal that this condition is satisfied when the distance between receiver and transmitter (or scatterer) exceeds a quarter of Rayleigh distance. The details of the proposed algorithm are explained in the following sections.

Notations: Random variables are displayed in sans serif, upright fonts; their realizations in serif, italic fonts. Vectors and matrices are denoted by bold lowercase and uppercase letters, respectively. The transpose, conjugate transpose, and complex conjugation are denoted by $(\cdot)^T$, $(\cdot)^H$, and $(\cdot)^*$. The inverse operation is denoted by $(\cdot)^{-1}$. The operator $\operatorname{diag}(\cdot)$ denotes the diagonal matrix whose diagonal elements are the elements of a given vector. The operator $\Re\{\cdot\}$ denotes the real part of a complex number. The operator $\|\cdot\|_2$ denotes l^2 norm. $N \times N$ identity matrix is denoted by I_N . The projection matrix of X is denoted by P_X , which equals $X(X^HX)^{-1}X^H$. A circularly-symmetric complex Gaussian random variable whose mean is μ and variance is σ^2 is denoted by $\mathcal{CN}(\mu, \sigma^2)$. The operator $\operatorname{arg}(\cdot)$ denotes the phase of the given value.

II. SYSTEM MODEL

Consider a base station $(2M_x + 1) \times (2M_z + 1)$ UPA, user equipment (UE) with a single omnidirectional antenna, and scatters in Fig. 1. Here, the UE transmits the orthogonal frequency division multiplexing (OFDM) pilot symbols

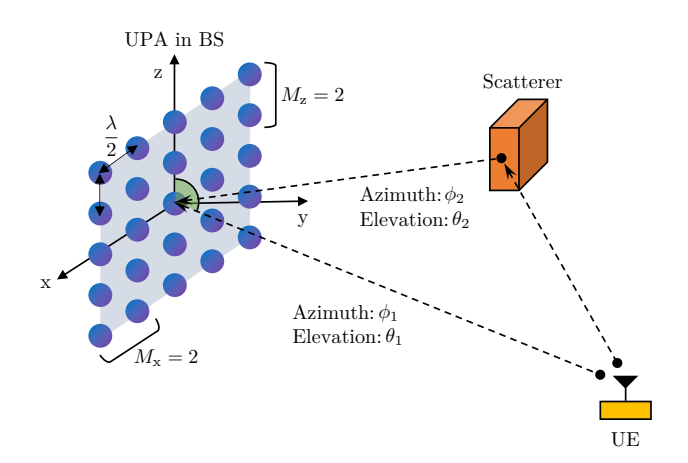


Figure 1. A graphical representation for the system model. In this figure, there are two signal paths, and the transmitter and all the scatterers are in NF. Both $M_{\rm x}$ and $M_{\rm z}$ are 2.

through K subcarriers, and the base station (BS) receives the pilot symbols. The BS is equipped with a hybrid beamformer with N radio frequency (RF) chains. In the UPA, the spacing between adjacent antennas is set to $\lambda/2$, where λ denotes the wavelength. The size of array is $M_{\rm x}\lambda\times M_{\rm z}\lambda$, and Rayleigh distance equals $2\lambda(M_{\rm x}^2+M_{\rm z}^2)$ [3]. The number of antennas, M, equals $(2M_{\rm x}+1)\times(2M_{\rm z}+1)$. The antenna in the center of the UPA is located in the origin, and all the antennas are located on the xz plane for notational convinience.

Letting d denote the distance between the center of the UPA and the UE (or one of the scatterers), the position of UE can be given by $[d\cos\phi\sin\theta, d\sin\phi\sin\theta, d\cos\theta]^T$. Here, ϕ and θ denote the azimuth and elevation of the signal impinging on the UPA. The distance between the m-the antenna and the UE, d_m , is given by

$$d_{m} \triangleq \left\| \left[p_{m}^{\mathbf{x}} \ 0 \ p_{m}^{\mathbf{z}} \right] - \left[d \cos \phi \sin \theta \ d \sin \phi \sin \theta \ d \cos \theta \right] \right\|_{2}$$

where $p_m^{\rm x}$ and $p_m^{\rm z}$ denote the x-coordinate and z-coordinate of the m-th antenna element. A NF steering vector $\boldsymbol{a}(\phi,\theta,d,f) \in \mathbb{C}^{M \times 1}$ is given by

$$\boldsymbol{a}(\phi, \theta, d, f) \triangleq \left[e^{j\frac{2\pi(d_1 - d)}{\lambda}} e^{j\frac{2\pi(d_2 - d)}{\lambda}} \cdots e^{j\frac{2\pi(d_M - d)}{\lambda}} \right]^T$$
 (2)

where f denotes the carrier frequency, which equals λc with c denoting the speed of light.

A channel vector at the k-th subcarrier, $\boldsymbol{h}^{(k)} \in \mathbb{C}^{M \times 1}$, is given by [16]

$$\boldsymbol{h}^{(k)} = \sum_{l=1}^{L} \alpha_{l} \boldsymbol{a}(\phi_{l}, \theta_{l}, d_{l}, f^{(k)}) e^{-j2\pi(k-1)\Delta_{f} \tau_{l}}$$
(3)

for $k=1,2,\ldots,K$, where L denotes the number of signal paths, and α_l , ϕ_l , θ_l , and τ_l respectively denote the complex channel gain, angle-of-arrival (AOA) azimuth, AOA elevation, and time-of-arrival (TOA) of the l-th signal path. If the line-of-sight (LOS) path exists, the first path denotes the LOS path. When the LOS path exists, d_1 denotes the distance between the transmitter and the center of the array, whereas d_l denotes

the distance between the (l-1)-th scatterer and the center of the array for $l=2,3,\ldots,L$.

Letting the pilot symbol be transmitted a total of P times, the p-th received pilot symbol at the k-th subcarrier, $\boldsymbol{x}_p^{(k)}$, can be represented as

$$\mathbf{x}_{p}^{(k)} = \mathbf{W}_{p}^{H} \mathbf{h}^{(k)} s_{p}^{(k)} + \mathbf{n}_{p}^{(k)}$$
 (4)

for $k=1,2,\ldots,K$ and $p=1,2,\ldots,P$, where $\mathbf{W}_p\in\mathbb{C}^{M\times N}$ denotes the combining matrix for the p-th pilot symbol, $s_p^{(k)}$ denotes the p-th pilot symbol at the k-th subcarrier, and $\mathbf{n}_p^{(k)}\in\mathbb{C}^{N\times 1}$ denotes the noise vector. Squared l^2 norm of each column of \mathbf{W}_p equals M/N. Each entry of $\mathbf{n}_p^{(k)}$ follows $\mathcal{CN}(0,\sigma^2)$, where, σ^2 denotes the power of the noise. From pilot symbols, $\mathbf{y}_p^{(k)}\in\mathbb{C}^{N\times 1}$ is drawn as

$$\mathbf{y}_{p}^{(k)} \triangleq \frac{\mathbf{x}_{p}^{(k)}(s_{p}^{(k)})^{*}}{\left|s_{p}^{(k)}\right|^{2}} = \mathbf{W}_{p}^{H}\mathbf{h}^{(k)} + \mathbf{v}_{p}^{(k)}$$
(5)

for $k=1,2,\ldots,K$ and $p=1,2,\ldots,P$, where $\mathbf{v}_p^{(k)}\triangleq\mathbf{n}_p^{(k)}(s_p^{(k)})^*/\big|s_p^{(k)}\big|^2$. In this paper, $\big|s_p^{(k)}\big|$ is set to 1 so that the power of the noise part in $\mathbf{y}_p^{(k)}$ remains to be σ^2 . Lastly, P received pilot symbols are organized as

$$\boldsymbol{y}^{(k)} \triangleq \left[(\boldsymbol{y}_1^{(k)})^T \ (\boldsymbol{y}_2^{(k)})^T \ \cdots \ (\boldsymbol{y}_P^{(k)})^T \right]^T$$
(6)

for $k=1,2,\ldots,K$, where $\boldsymbol{y}^{(k)}\in\mathbb{C}^{NP\times 1}$ denotes organized pilot symbols at the k-th subcarrier. $\boldsymbol{y}^{(k)}$ can be alternatively represented as

$$\boldsymbol{y}^{(k)} = \boldsymbol{W}^{H} \boldsymbol{h}^{(k)} + \boldsymbol{\mathsf{v}}^{(k)} \tag{7}$$

where $\boldsymbol{W} \triangleq [\boldsymbol{W}_1 \, \boldsymbol{W}_2 \cdots \boldsymbol{W}_P] \in \mathbb{C}^{M \times NP}$ and $\boldsymbol{\mathbf{v}}^{(k)} \triangleq [(\boldsymbol{\mathbf{v}}_1^{(k)})^T \, (\boldsymbol{\mathbf{v}}_2^{(k)})^T \cdots (\boldsymbol{\mathbf{v}}_P^{(k)})^T]^T$.

According to (7), there are a total of NPK entries, and the total of noise power equals $\sigma^2 NPK$. Thus, the signal-to-noise ratio (SNR), γ , is defined as

$$\gamma \triangleq 10 \log \left(\frac{\sum_{k=1}^{K} \| \boldsymbol{W}^{H} \boldsymbol{h}^{(k)} \|_{2}^{2}}{\sigma^{2} NPK} \right) \text{ [dB]}.$$
 (8)

III. PROPOSED NF ANGLE AND RANGE ESTIMATION ALGORITHM FOR UPA

In this section, we introduce the NF angle and range algorithm that significantly reduces the computational complexity by decoupling the 3D search into a series of 2D search and 1D search. Moreover, we derive the condition that guarantees the accurate estimation of the proposed algorithm.

A. Condition for Lower-dimensional Search-based Estimation in Near-field

Letting $G_{\rm a}$, $G_{\rm e}$, and $G_{\rm d}$ respectively denote the number of discretized azimuths, elevations, and distances for searching, the sets of candidate azimuths, elevations, and distances can be given by

$$S_{\mathbf{a}} \triangleq \left\{ 1 \frac{180^{\circ}}{G_{\mathbf{a}}}, 2 \frac{180^{\circ}}{G_{\mathbf{a}}}, \dots, G_{\mathbf{a}} \frac{180^{\circ}}{G_{\mathbf{a}}} \right\} \tag{9}$$

$$S_{\rm e} \triangleq \left\{ 1 \frac{180^{\circ}}{G_{\rm e}}, 2 \frac{180^{\circ}}{G_{\rm e}}, \dots, G_{\rm e} \frac{180^{\circ}}{G_{\rm e}} \right\}$$
 (10)

$$S_{d} \triangleq \left\{1 \frac{d_{\text{max}}}{G_{d}}, 2 \frac{d_{\text{max}}}{G_{d}}, \dots, G_{d} \frac{d_{\text{max}}}{G_{d}}\right\}$$
(11)

where $S_{\rm a}$, $S_{\rm e}$, and $S_{\rm d}$ respectively denote the set of discretized azimuths, elevations, and distances. The maximum searching distance is denoted by $d_{\rm max}$. Generally, $d_{\rm max}$ is set to Rayleigh distance [9]–[11].

The proposed algorithm first estimates the azimuth and elevation with a 2D search. During the 2D search, the searching distance is fixed. This 2D search-based azimuth and elevation estimation can be represented as

$$\left\{\hat{\phi}_{2D}, \hat{\theta}_{2D}\right\} = \underset{\substack{\phi \in \mathcal{S}_{a}, \\ \theta \in \mathcal{S}_{e}}}{\operatorname{argmax}} \sum_{k=1}^{K} \left| \left(\boldsymbol{W}^{H} \boldsymbol{a}(\phi, \theta, d_{f}, f^{(k)}) \right)^{H} \boldsymbol{y}^{(k)} \right|^{2}$$
(12)

where $\hat{\phi}_{2\mathrm{D}}$ and $\hat{\theta}_{2\mathrm{D}}$ denote the azimuth and elevation estimated by 2D search, and d_{f} denotes the fixed constant for the distance. We set d_{f} to a sufficiently large value (e.g., infinity), such that the NF steering vector in (12) becomes the FF steering vector. Letting $\boldsymbol{b}(\phi,\theta,f) \in \mathbb{C}^{M\times 1}$ denotes the FF steering vector, the m-th element of $\boldsymbol{b}(\phi,\theta,f)$ can be given by

$$\boldsymbol{b}_{m}(\phi, \theta, f) \triangleq e^{-j\frac{2\pi}{\lambda}(p_{m}^{x}\cos\phi\sin\theta + p_{m}^{z}\cos\theta)}.$$
 (13)

With the FF steering vector, (12) can be rewritten as

$$\left\{\hat{\phi}_{2D}, \hat{\theta}_{2D}\right\} = \underset{\substack{\phi \in \mathcal{S}_{a}, \\ \theta \in \mathcal{S}_{e}}}{\operatorname{argmax}} \sum_{k=1}^{K} \left| \left(\boldsymbol{W}^{H} \boldsymbol{b}(\phi, \theta, f^{(k)}) \right)^{H} \boldsymbol{y}^{(k)} \right|^{2}.$$

However, to guarantee that the 2D search estimates the azimuth and elevation accurately, it must be proved that the objective function in (14) is maximized only when $\hat{\phi}_{\rm 2D}$ and $\hat{\theta}_{\rm 2D}$ equals one of the true azimuths and elevations. Otherwise, the results of the 2D search may have bias even under ideal environments (e.g., noiseless environments). For the derivation, we consider that the NF steering vectors for all signal paths are orthogonal to each other since M is large. In this case, each signal path does not affect the estimation of azimuths and elevations of other paths. Also, the errors induced by the discretized grid and the noise are not considered in this derivation.

Letting $\bar{\phi}$, $\bar{\theta}$, and \bar{d} respectively denote the azimuth, elevation, and distance of the strongest signal path, the objective function in (14), $|\boldsymbol{b}(\phi,\theta,f^{(k)})^H \boldsymbol{W} \boldsymbol{W}^H \boldsymbol{a}(\bar{\phi},\bar{\theta},\bar{d},f^{(k)})|^2$, must be maximized only when $\phi = \bar{\phi}$ and $\theta = \bar{\theta}$. We first design \boldsymbol{W} that satisfies $\boldsymbol{W} \boldsymbol{W}^H = P \boldsymbol{I}_M$. Then, $\boldsymbol{W} \boldsymbol{W}^H$ becomes a constant, so the objective function in (14) reaches the maximum when $|\boldsymbol{b}(\phi,\theta,f^{(k)})^H \boldsymbol{a}(\bar{\phi},\bar{\theta},\bar{d},f^{(k)})|^2$ is maximized. If the condition in the following theorem is satis-

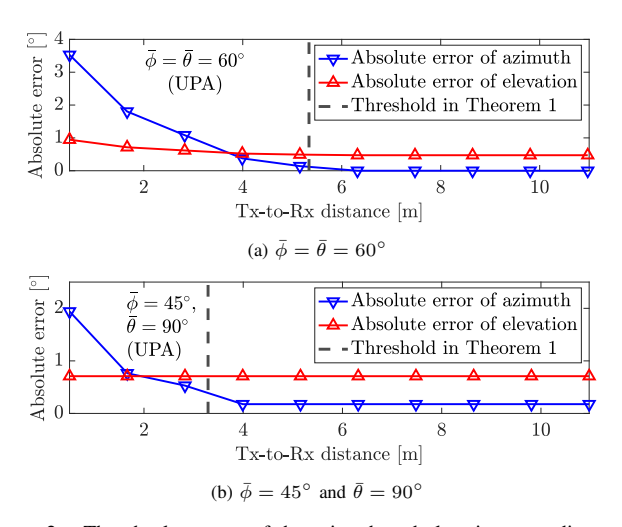


Figure 2. The absolute error of the azimuth and elevation according to the distance between BS and UE. The black dotted line denotes the threshold in Theorem 1.

fied, $\left| {m b}(\phi, \theta, f^{(k)})^H {m a}(\bar{\phi}, \bar{\theta}, \bar{d}, f^{(k)}) \right|^2$ becomes maximum only when $\phi = \bar{\phi}$ and $\theta = \bar{\theta}$.

Theorem 1. If $\bar{d} \geq \frac{\lambda}{2} [(M_x | \cos \bar{\phi} \cos \bar{\theta}| + M_z | \sin \bar{\theta}|)^2 + (M_x \sin \bar{\phi})^2]$, the azimuth and elevation estimated by the 2D search are guaranteed to be the true azimuth and elevation when there is no additive noise.

Proof. See Appendix A.
$$\Box$$

Theorem 1 shows the 2D search-based estimation is guaranteed to be accurate when the distance between the UE (or scatterer) and the BS exceeds the specified threshold. The threshold in the theorem approaches maximum when $\bar{\phi} = \bar{\theta} = 90^{\circ}$, which means that the transmitter (or scatterer) is located at the front of the receiver. In this case, the threshold equals to $\lambda (M_{\rm x}^2 + M_{\rm z}^2)/2$, which is the quarter of Rayleigh distance. To illustrate the insight of Theorem 1, numerical results are presented in Fig. 2. In these results, there is no noise, and only a LOS path between BS and UE exists. $M_{\rm x}$ and M_z are respectively set to 64 and 32. Fig. 2 shows that the absolute error of both azimuth and elevation reaches the minimum when the distance is larger than the threshold in Theorem 1, which changes according to azimuth and elevation. Exceptionally, the elevation estimation is less affected by the distance if the elevation is close to 90°. This result also illustrates that conducting a 3D dimensional search outside the established threshold is not required.

B. Sequential Angle and Distance Estimation with Greedy Algorithm

In this section, we introduce the computationally efficient estimation algorithm, considering AOA and distance of every signal path satisfy the condition in Theorem 1.² The proposed

 $^{^{1}}$ To satisfy this condition, NP has to be equal to or greater than M, and this may cause the large overhead for collecting measurements. To reduce the overhead, a beamwidth widening strategy that deactivates the part of the array can be exploited [17]. However, this strategy reduces the Rayleigh distance since it only uses a part of the array. In fully digital beamformers, designing W does not need to be considered.

²In practice, the equipment with a large antenna array (e.g., BS) is located in a high place, so satisfying the condition may not be a major issue. If an accurate estimation of the angles and distances that do not satisfy the theorem is required, a 3D search can be conducted on a range within the threshold in the theorem.

algorithm first estimates the azimuth and elevation by a 2D search. Then, the distance is estimated by the 1D search on the distance axis, with the searching angle fixed to the previously estimated azimuth and elevation.

Letting $\mathbf{z}_{l}^{(k)}$ denotes the vector for the k-th subcarrier that is used in the l-th iteration, the l-th AOA is estimated as

$$\left\{\hat{\phi}_{l}, \hat{\theta}_{l}\right\} = \underset{\substack{\phi \in \mathcal{S}_{a}, \\ \theta \in \mathcal{S}_{a}}}{\operatorname{argmax}} \sum_{k=1}^{K} \left| \left(\boldsymbol{W}^{H} \boldsymbol{b}(\phi, \theta, f^{(k)}) \right)^{H} \boldsymbol{z}_{l}^{(k)} \right|^{2}$$
(15)

where $\hat{\phi}_l$ and $\hat{\theta}_l$ denotes the l-th estimated azimuth and elevation. In the initial iteration, $\mathbf{z}_1^{(k)}$ equals $\mathbf{y}^{(k)}$ for $k=1,2,\ldots,K$. After obtaining $\hat{\phi}_l$ and $\hat{\theta}_l$, the l-th distance is estimated as

$$\hat{d}_{l} = \underset{d \in \mathcal{S}_{d}}{\operatorname{argmax}} \sum_{k=1}^{K} \left| \left(\boldsymbol{W}^{H} \boldsymbol{a}(\hat{\phi}_{l}, \hat{\theta}_{l}, d, f^{(k)}) \right)^{H} \boldsymbol{z}_{l}^{k} \right|^{2}$$
(16)

where \hat{d}_l denotes the *l*-th estimated distance.

The components of all the estimated AOAs and distances that are previously estimated are subtracted from $\boldsymbol{z}_l^{(k)}$. Note that this subtraction is similar to that of orthogonal matching pursuit (OMP) [18]. The bases over which $\boldsymbol{z}_l^{(k)}$ is projected on, $\boldsymbol{\Lambda}_l^{(k)} \in \mathbb{C}^{NP \times l}$, is represented as

$$\mathbf{\Lambda}_{l}^{(k)} \triangleq \mathbf{W}^{H} \left[\mathbf{a} \left(\hat{\phi}_{1}, \hat{\theta}_{1}, \hat{d}_{1}, f^{(k)} \right) \mathbf{a} \left(\hat{\phi}_{2}, \hat{\theta}_{2}, \hat{d}_{2}, f^{(k)} \right) \right.$$

$$\cdots \mathbf{a} \left(\hat{\phi}_{l}, \hat{\theta}_{l}, \hat{d}_{l}, f^{(k)} \right) \right]. \quad (17)$$

For the next iteration, $z_{l+1}^{(k)}$ is set to

$$\boldsymbol{z}_{l+1}^{(k)} \triangleq (\boldsymbol{I}_{NP} - \boldsymbol{P}_{\boldsymbol{\Lambda}^{(k)}}) \boldsymbol{z}_{l}^{(k)}$$
(18)

for $k=1,2,\ldots,K$. A process from (15) to (18) denotes one iteration. Considering that L is already estimated, all the AOAs and distances can be estimated by L iterations. The computational complexity of the proposed AOA and distance estimation is $\mathcal{O}(LNPK(G_{\mathrm{a}}G_{\mathrm{e}}+G_{\mathrm{d}}))$. Reminding that G_{a} , G_{e} , and G_{d} is set proportional to M [20], the complexity of the proposed algorithm is much lower than $\mathcal{O}(LNPKG_{\mathrm{a}}G_{\mathrm{e}}G_{\mathrm{d}})$, the complexity of 3D search-based algorithm [11].

IV. SIMULATION RESULTS AND DISCUSSIONS

For the simulation, the center frequency f is set to $140\,\mathrm{GHz}$. M_x and M_z are respectively set to 64 and 32 so that $M=129\times65$. In this setting, Rayleigh distance equals $21.94\,\mathrm{m}$. The number of RF chains and the number of pilot symbols, N and P, are set to 64 and 132. The combining matrix $\mathbf{W}\in\mathbb{C}^{M\times NP}$ is set as any M columns of $NP\times NP$ 2D-discrete Fourier transform (DFT) matrix [21]. The number of signal paths L is set to 3, which is comprised of one LOS path and two

Table I. Computational complexity and average computation time of all algorithms

	Computational complexity	Average computation time
Proposed	$\mathcal{O}\left(LNPK\left(G_{\mathrm{a}}G_{\mathrm{e}}+G_{\mathrm{d}}\right)\right)$	19.57 seconds
3D-OMP [11]	$\mathcal{O}\left(LNPKG_{\mathrm{a}}G_{\mathrm{e}}G_{\mathrm{d}}\right)$	200.5 seconds
DS-OMP [14]	$\mathcal{O}(LNPK(M_{ m z}G_{ m e}G_{ m d} \ + MG_{ m a}))$	1.39 seconds

NLOS paths. Subcarrier spacing $\Delta_{\rm f}$ is set to 960 kHz. The number of subcarriers K is set low at 5 due to the excessive computation time. All azimuths, elevations, and distances are set according to the coordinates of the BS, UE, and scatterers. The coordinate of the BS is fixed to [0,0,3] m. However, the coordinates of the UE and scatterers are set differently for each simulation. The number of discretized azimuths, elevations, and distances, $G_{\rm a}$, $G_{\rm e}$, and $G_{\rm d}$, are set to $4M_{\rm x}$, $4M_{\rm z}$, and $8M_{\rm x}$, respectively. For root-mean-square error (RMSE) calculation, 200 Monte Carlo trials are conducted, and Intel i5-13600KF CPU (3.50 GHz) and 32 GB RAM are used in this simulation.

For the performance evaluation, the proposed algorithm is compared with 3D-OMP [11] and DS-OMP [14]. In [11], azimuth, elevation, and distance are estimated via 3D search. which is the most time-consuming among all algorithms. In [14], azimuth, elevation, and distance are estimated in a more efficient manner. To prevent excessive computation, $G_{\rm a},~G_{\rm e},~{\rm and}~G_{\rm d}$ are set to $M_{\rm x},~M_{\rm z},~{\rm and}~M_{\rm x}$ only for the simulation of 3D-OMP [11]. The computational complexity and average computation time of all algorithms are summarized in Table I. Although the grid size is set large for the proposed algorithm and DS-OMP [14], the average computation of the proposed algorithm and DS-OMP [14] are 19.57 seconds and 1.39 seconds, which are much smaller than the average computation of 3D-OMP [11], 200.5 seconds. This result shows that the actual computation time follows the trend of the computational complexity.

Fig. 3 shows the RMSE of azimuth, elevation, and distance versus the SNR. In this simulation, the distance between BS and UE is set to 15 m, and the distances between BS and scatterers are randomly set between [5, 15] m. The zcoordinate of UE and scatterers is fixed to 0. The azimuths of all signal paths are randomly set between [30°, 150°], and the elevations are determined based on the height of UE and scatterers. In Fig. 3, the proposed algorithm has the lowest RMSE in all ranges of SNR, and there is a reason. First, DS-OMP [14] employs only one column of UPA for elevation and distance estimation. Although this reduces the computational complexity, the algorithm becomes less robust to noise. The high RMSE of 3D-OMP [11] is mainly due to the sparse search. On the other hand, the proposed algorithm can reduce the complexity while leveraging the entire array. For this reason, the proposed algorithm can be considered as an option with the best accuracy-complexity trade-off.

Fig. 4 shows the RMSE of azimuth, elevation, and distance versus the distance. In this simulation, the SNR is set to 10 dB, and the distance between BS and UE (and scatterers) is set

 $^{^3}$ The number of signal paths can be estimated by counting large singular values of the matrix whose k-th column is $h^{(k)}$. For the counting, criteria such as minimum description length (MDL) and Akaike information criterion (AIC) can be exploited [19]. On the other hand, we can set the threshold to determine the end of the iteration in a way that many compressive sensing (CS) techniques do.

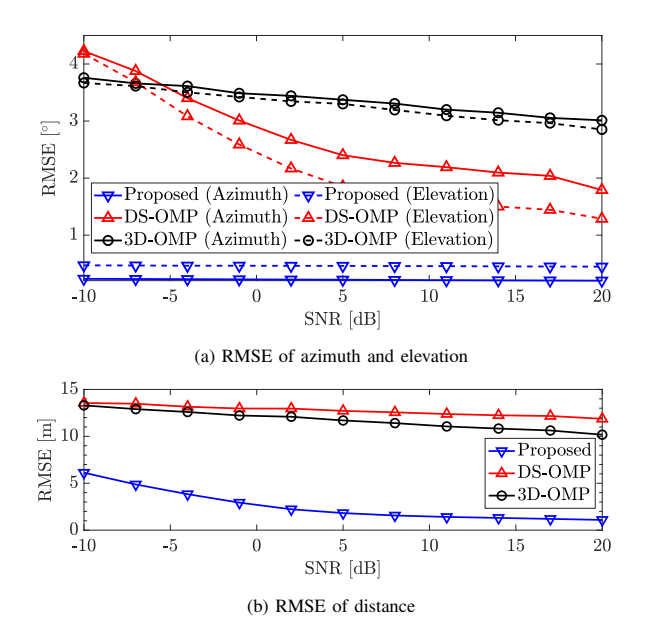


Figure 3. The RMSE of the azimuth, elevation, and distance versus SNR.

according to the x-axis in Fig. 4 (1 m to 31 m). The azimuths of all signal paths are randomly set between [30°, 150°], and the elevations are randomly set between [90°, 180°]. In Fig. 4a, the RMSE of azimuth and elevation of the proposed algorithm is high in the close distance due to Theorem 1. On the other hand, the angle estimation of 3D-OMP [11] is not affected by distance. Interestingly, the RMSE of DS-OMP [14], which also decouples 3D search, is also inversely proportional to the distance. In Fig. 4b, the accuracy of distance estimation is inversely proportional to distance. This is because the curvature of the wavefront is more distinct when the BS and UE are close. However, the RMSE of the proposed algorithm increases at a close distance since an erroneously estimated angle affects the following 1D distance estimation. Nonetheless, the distance estimation of the proposed algorithm is more accurate than the others if the distance is larger than 1 m.

V. CONCLUSION

In this paper, we presented a computationally efficient angle and distance estimation algorithm for extremely large UPA systems. To reduce computation, the proposed algorithm decouples the original 3D search-based azimuth, elevation, and distance estimation into a series of 2D search-based azimuth and elevation estimation and 1D search-based distance estimation. We revealed that the estimation of the proposed algorithm is accurate when the UE (or scatterers) move away from the BS beyond a certain threshold, which is around a quarter of Rayleigh distance in UPA systems. This finding shows that a high-dimensional search for angle and distance estimation is unnecessary except when the UE (or scatterers) exists in a region close to BS. The simulation results show that the proposed algorithm has a superior accuracy-complexity trade-off compared to existing works. The findings in this

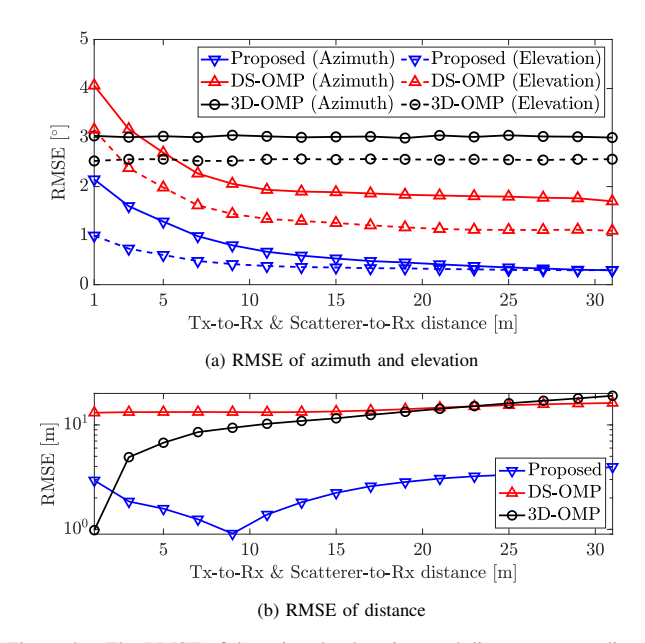


Figure 4. The RMSE of the azimuth, elevation, and distance versus distance.

paper envision faster communication, positioning, and sensing in the NF and can provide a guideline for designing systems with large array antennas.

APPENDIX A PROOF OF THEOREM 1

With Fresnel approximation, the exponent of the m-th element of the NF steering vector is approximated as

$$\ln\left(\boldsymbol{a}_{m}(\phi,\theta,d,f)\right) = j\frac{2\pi}{\lambda}\left[-\left(p_{m}^{x}\cos\phi\sin\theta + p_{m}^{z}\cos\theta\right) + \frac{1}{2d}\left\{\left(p_{m}^{x}\cos\phi\cos\theta - p_{m}^{z}\sin\theta\right)^{2} + \left(p_{m}^{x}\sin\phi\right)^{2}\right\}\right]. (19)$$

Using the approximation in (19), the square of the correlation between the FF steering vector and the NF steering vector, $|\boldsymbol{b}(\phi,\theta,f)^H\boldsymbol{a}(\bar{\phi},\bar{\theta},\bar{d},f)|^2$, then is approximated as

$$\begin{aligned} \left| \boldsymbol{b}(\phi, \theta, f)^{H} \boldsymbol{a}(\bar{\phi}, \bar{\theta}, \bar{d}, f) \right|^{2} \\ &\approx \left| \sum_{m=1}^{M} e^{j\frac{2\pi}{\lambda} \frac{(p_{m}^{\mathbf{x}} \cos \bar{\phi} \cos \bar{\theta} - p_{m}^{\mathbf{z}} \sin \bar{\theta})^{2} + (p_{m}^{\mathbf{x}} \sin \bar{\phi})^{2}}{2\bar{d}}} \times \right. \\ &\left. e^{j\frac{2\pi}{\lambda} \left[(p_{m}^{\mathbf{x}} \cos \phi \sin \theta + p_{m}^{\mathbf{z}} \cos \theta) - (p_{m}^{\mathbf{x}} \cos \bar{\phi} \sin \bar{\theta} + p_{m}^{\mathbf{z}} \cos \bar{\theta}) \right]} \right|^{2} (20) \end{aligned}$$

In this appendix, we verify if the approximated correlation in (20) is maximized when $\theta = \bar{\theta}$. For notational convinience, we introduce variables A_m and B_m , which are denoted by

$$A_{m} \triangleq e^{j\frac{2\pi}{\lambda}} \frac{(p_{m}^{\mathbf{x}}\cos\bar{\phi}\cos\bar{\theta} - p_{m}^{\mathbf{z}}\sin\bar{\theta})^{2} + (p_{m}^{\mathbf{x}}\sin\bar{\phi})^{2}}{2\bar{d}}$$

$$B_{m} \triangleq e^{j\frac{2\pi}{\lambda}} [(p_{m}^{\mathbf{x}}\cos\phi\sin\theta + p_{m}^{\mathbf{z}}\cos\theta) - (p_{m}^{\mathbf{x}}\cos\bar{\phi}\sin\bar{\theta} + p_{m}^{\mathbf{z}}\cos\bar{\theta})]$$
(21)

for $m=1,2,\ldots,M.$ When the (M+1)/2-th antenna is placed at the center, $A_m=A_{M-m+1}$ and $B_m=B_{M-m+1}^*$

for $m=1,2,\ldots,(M-1)/2$. With this symmetric property, $|\boldsymbol{b}(\phi,\theta,f)^H\boldsymbol{a}(\bar{\phi},\bar{\theta},\bar{d},f)|^2$ can be simply represented as

$$\begin{aligned} \left| \boldsymbol{b}(\phi, \theta, f)^{H} \boldsymbol{a}(\bar{\phi}, \bar{\theta}, \bar{d}, f) \right|^{2} \\ &= 1 + \left| \sum_{m=1}^{\frac{M-1}{2}} 2A_{m} \Re\{B_{m}\} \right|^{2} \\ &= 1 + \left\{ \sum_{m=1}^{\frac{M-1}{2}} 2A_{m} \Re\{B_{m}\} \right\} \left\{ \sum_{m=1}^{\frac{M-1}{2}} 2A_{m}^{*} \Re\{B_{m}\} \right\} \\ &= 1 + \sum_{n=1}^{\frac{M-1}{2}} \sum_{m=1}^{\frac{M-1}{2}} 4A_{m} A_{n}^{*} \Re\{B_{m}\} \Re\{B_{n}\} \\ &= 1 + \sum_{n=1}^{\frac{M-1}{2}} \sum_{m=1}^{\frac{M-1}{2}} 4\Re\{A_{m} A_{n}^{*}\} \Re\{B_{m}\} \Re\{B_{n}\}. \end{aligned} (23)$$

The first approximation in (23) equals to the approximation made in (20). $\Re\{A_mA_n^*\}$ is a constant since ϕ and θ are the only variables that change. $\Re\{B_m\}$ and $\Re\{B_n\}$ are variables between -1 and 1, where they are maximized when θ is $\bar{\theta}$.

The organized representation in (23) tells that $\left| \boldsymbol{b}(\phi,\theta,f)^H \boldsymbol{a}(\bar{\phi},\bar{\theta},\bar{d},f) \right|^2$ is maximized if following conditions are satisfied. These conditions are:

- the part affected by ϕ and θ , $\Re\{B_m\}\Re\{B_n\}$, is a maximum value for m, n = 1, 2, ..., (M-1)/2; and
- the constant part, $\Re\{A_mA_n^*\}$, is a positive value for $m, n = 1, 2, \dots, (M-1)/2$.

However, note that these are sufficient conditions for maximizing $\left| \boldsymbol{b}(\phi,\theta,f)^H \boldsymbol{a}(\bar{\phi},\bar{\theta},\bar{d},f) \right|^2$. For all possible combinations of m and n, $\Re\{B_m\}\Re\{B_n\}$ is maximized to 1 when $\phi=\bar{\phi}$ and $\theta=\bar{\theta}$. $\Re\{A_mA_n^*\}$ is a positive value when the phase of the complex value, $\arg(A_mA_n^*)$, is between $-\pi/2$ and $\pi/2$. According to (20), $\left|\arg(A_mA_n^*)\right|$ is maximized when the m-th antenna is one of the antennas in the corner of the UPA and n=(M-1)/2. If this maximum phase difference is smaller than $\pi/2$, $\Re\{A_mA_n^*\}$ is always a positive value. The maximum phase difference between A_m and A_n can be represented as

$$\max_{m,n=1,2,...,\frac{M-1}{2}} |\arg(A_m A_n^*)|$$

$$= \frac{\pi \lambda \left[(M_x | \cos \bar{\phi} \cos \bar{\theta} | + M_z | \sin \bar{\theta} |)^2 + (M_x \sin \bar{\phi})^2 \right]}{4\bar{d}}.(24)$$

The condition that satisfies $\max \left| \arg(A_m A_n^*) \right| \leq \pi/2$ is

$$\bar{d} \ge \frac{\lambda}{2} \left[(M_{\rm x} | \cos \bar{\phi} \cos \bar{\theta} | + M_{\rm z} | \sin \bar{\theta} |)^2 + (M_{\rm x} \sin \bar{\phi})^2 \right] \tag{25}$$

where this is the condition in Theorem 1.

REFERENCES

- W. Saad, M. Bennis, and M. Chen, "A vision of 6G wireless systems: Applications, trends, technologies, and open research problems," *IEEE Netw.*, vol. 34, pp. 134–142, May 2020.
- [2] I. F. Akyildiz and J. M. Jornet, "Realizing ultra-massive MIMO (1024×1024) communication in the (0.06–10) terahertz band," *Nano Commun. Netw.*, vol. 8, pp. 46–54, Jun. 2016.
- [3] K. T. Selvan and R. Janaswamy, "Fraunhofer and Fresnel distances: Unified derivation for aperture antennas," *IEEE Antennas Propag. Mag.*, vol. 59, pp. 12–15, Aug. 2017.

- [4] M. Z. Win, A. Conti, S. Mazuelas, Y. Shen, W. M. Gifford, D. Dardari, and M. Chiani, "Network localization and navigation via cooperation," *IEEE Commun. Mag.*, vol. 49, pp. 56–62, May 2011.
- [5] A. Conti, F. Morselli, Z. Liu, S. Bartoletti, S. Mazuelas, W. C. Lindsey, and M. Z. Win, "Location awareness in beyond 5G networks," *IEEE Commun. Mag.*, vol. 59, pp. 22–27, Nov. 2021. special issue on *Location Awareness for 5G and Beyond*.
- [6] M. Z. Win, Y. Shen, and W. Dai, "A theoretical foundation of network localization and navigation," *Proc. IEEE*, vol. 106, pp. 1136–1165, July 2018. special issue on *Foundations and Trends in Localization Technologies*.
- [7] A. Conti, S. Mazuelas, S. Bartoletti, W. C. Lindsey, and M. Z. Win, "Soft information for localization-of-things," *Proc. IEEE*, vol. 107, pp. 2240– 2264. Nov. 2019.
- [8] G. Torsoli, M. Z. Win, and A. Conti, "Blockage intelligence in complex environments for beyond 5G localization," *IEEE J. Sel. Areas Commun.*, vol. 41, pp. 1688–1701, June 2023. special issue on *3GPP Technologies:* 5G-Advanced and Beyond.
- [9] M. Cui and L. Dai, "Channel estimation for extremely large-scale MIMO: Far-field or near-field?," *IEEE Trans. Commun.*, vol. 70, pp. 2663–2677, Apr. 2022.
- [10] Y. Lu and L. Dai, "Near-field channel estimation in mixed LoS/NLoS environments for extremely large-scale MIMO systems," *IEEE Trans. Commun.*, vol. 71, pp. 3694–3707, Mar. 2023.
- [11] Z. Lu, Y. Han, S. Jin, and M. Matthaiou, "Near-field localization and channel reconstruction for ELAA systems," *IEEE Trans. Wireless Commun.*, vol. 23, pp. 6938–6953, Dec. 2024.
- [12] N. Yuen and B. Friedlander, "Performance analysis of higher order ESPRIT for localization of near-field sources," *IEEE Trans. Signal Process.*, vol. 46, pp. 709–719, Mar. 1998.
- [13] C. Huang, J. Xu, W. Xu, X. You, C. Yuen, and Y. Chen, "Low-complexity channel estimation for extremely large-scale MIMO in near field," *IEEE Wireless Commun. Lett.*, vol. 13, pp. 671–675, Mar. 2024.
- [14] X. Peng, L. Zhao, Y. Jiang, and J. Liu, "Channel estimation for UPA-assisted near-field channel in extremely large-scale massive MIMO systems," in *Proc. IEEE Int. Conf. Commun.*, pp. 738–743, Jun. 2024.
- [15] Y. Yin et al., "A 37–42-GHz 8 × 8 phased-array with 48–51-dBm EIRP, 64–QAM 30-Gb/s data rates, and EVM analysis versus channel RMS errors," *IEEE Trans. Microw. Theory Techn.*, vol. 68, pp. 4753–4764, Nov. 2020.
- [16] A. M. Elbir, W. Shi, A. K. Papazafeiropoulos, P. Kourtessis, and S. Chatzinotas, "Near-field terahertz communications: Model-based and model-free channel estimation," *IEEE Access*, vol. 11, pp. 36409–36420, Apr. 2023.
- [17] H. Chung, S. Hong, and S. Kim, "Efficient multi-user channel estimation for RIS-aided mmWave systems using shared channel subspace," *IEEE Trans. Wireless Commun.*, vol. 23, pp. 8512–8527, Aug. 2024.
- [18] T. T. Cai and L. Wang, "Orthogonal matching pursuit for sparse signal recovery with noise," *IEEE Trans. Inf. Theory*, vol. 57, pp. 4680–4688, Jun. 2011.
- [19] M. Wax and T. Kailath, "Detection of signals by information theoretic criteria," *IEEE Trans. Acoust., Speech, Signal Process.*, vol. 33, pp. 387–392, Apr. 1985.
- [20] M. Cui, Z. Wu, Y. Lu, X. Wei, and L. Dai, "Near-field MIMO communications for 6G: Fundamentals, challenges, potentials, and future directions," *IEEE Commun. Mag.*, vol. 61, pp. 40–46, Jan. 2023.
- [21] A. Sayeed and N. Behdad, "Continuous aperture phased mimo: Basic theory and applications," in *Proc. Allerton Conf. on Commun., Control, and Comput.*, pp. 1196–1203, Oct. 2010.